LBL-15189
Preprint

Lawrence Berkeley Laboratory
UNIVERSITY OF CALIFORNIA

ENERGY & ENVIRONMENT
DIVISION

To be published as a chapter in the Monograph Volume,
LITHIUM BATTERY TECHNOLOGY, Ed. H.V. Venkatasetty,
Wiley Interscience Publishers, New York, (in press)

HIGH-TEMPERATURE LITHIUM BATTERIES

E.J. Cairns

October 1982

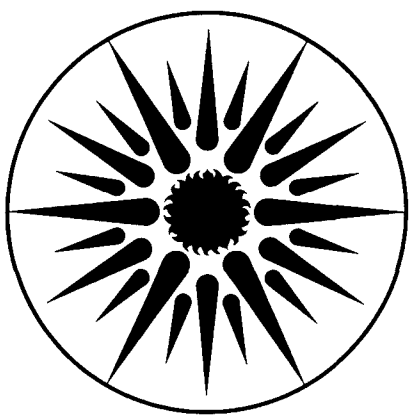

**ENERGY
AND ENVIRONMENT
DIVISION**

Prepared for the U.S. Department of Energy under Contract DE-AC03-76SF00098

DISCLAIMER

LBL-15189

HIGH-TEMPERATURE LITHIUM BATTERIES

Elton J. Cairns
Lawrence Berkeley Laboratory, and
University of California
Berkeley, California 94720

in

LITHIUM BATTERY TECHNOLOGY

H. V. Venkatasetty, ed.

Wiley Interscience Publishers
New York, NY

(in press)

This work was supported by the U.S. Department of Energy
under Contract DE-AC03-76SF00098.

HIGH-TEMPERATURE LITHIUM BATTERIES

Elton J. Cairns
Lawrence Berkeley Laboratory, and
University of California
Berkeley, California 94720

I. Introduction

It is clear from a perusal of the other chapters in this volume that lithium cells and batteries generally offer very high specific energy (over 100 Wh/kg in most cases), a distinct advantage over other types of cells. Rechargeable lithium cells that operate at ambient temperature have been very difficult to develop because of the problems associated with the repeated deposition of lithium in a compact, porous, active form (no dendrites or permanent passivation), and because of the scarcity of lithium-compatible positive electrode reactants that undergo reversible electrode reactions (in lithium-compatible electrolytes). In addition, high specific power has been difficult to achieve in rechargeable ambient-temperature lithium cells because of the low ionic conductivity of the available non-aqueous electrolytes. It has been found that a number of these problems can be circumvented by the use of rechargeable lithium cells that operate at elevated temperatures (300-500°C).

Some of the advantages gained by the use of high-temperature lithium cells include faster electrode reactions, faster transport processes (diffusion, migration), higher ionic conductivities, and faster equilibration among the various reactants and products. These properties help make it possible to achieve specific energies well above 100 Wh/kg, specific powers well above 100 W/kg, and cycle lives of 300-1500 deep cycles.

The specific-energy advantage offered by rechargeable lithium cells, as compared to other rechargeable cells can be seen by means of a comparison of theoretical specific energies. The theoretical specific energy of a cell can be calculated from tabulated free energy of formation data, provided that the

overall cell reaction is known.

$$\text{Theoretical specific energy} = \frac{-\Delta G}{\Sigma \gamma_i M_i} \qquad (1)$$

where ΔG is the Gibbs free energy change for the overall cell reaction, γ_i is the number of moles of reactant i and M_i is the molecular weight of reactant i. It is clear from Equation 1 that large (negative) values of ΔG and small values of M_i are necessary for high theoretical specific energies. Figure 1 shows the theoretical specific energy points for a number of rechargeable cells, and lines of constant cell voltage, as labeled.[1] Notice that most of the points in Figure 1 showing the highest theoretical specific energy are for cells with lithium or sodium negative electrodes (because of the low electronegativity and low equivalent weight of lithium and sodium).

The advantages cited above are accompanied by certain disadvantages, including the inconvenience of elevated-temperature operation, and more severe corrosion problems. These, and other specific problems will be discussed below in the sections that deal with the individual types of cells.

In the search for electrolytes that are compatible with lithium and various positive electrode reactants at elevated temperatures, it has been found that a number of lithium halide-alkali halide molten salt mixtures are thermodynamically stable with respect to lithium metal and various positive electrode reactants, and are highly conductive of lithium ions.[2] This has resulted in research and development of various lithium cells discussed in the next sections of this chapter. A significant search has been made for solid lithium-ion-conducting electrolytes stable to elemental lithium. Only a few such electrolytes have been found such as LiI and Li_3N. Many other lithium-ion conductors, including lithium halide-containing glasses are known, but they are not stable to lithium metal. This topic is reviewed by Huggins elsewhere in this volume.

II. Lithium Cells with Molten-Salt Electrolytes

A. Lithium/Halogen and Lithium/Chalcogen Cells.

Based upon purely thermodynamic considerations, there are many elements and compounds which could be used as positive electrodes in conjunction with lithium negative electrodes to yield a cell of high specific energy. Other considerations cause the range of choices to be narrowed to the few systems discussed in detail below. For example, a Li/F_2 cell would provide about 6 V, and 6200 W-h/kg theoretical specific energy. However, the difficulties of providing an electrolyte having sufficient stability, and of providing a stable fluorine electrode are formidable. A good deal of work has been performed on Li/Cl_2 cells (theoretical specific energy = 2200 Wh/kg) using a molten LiCl electrolyte, and a chlorine electrode of porous carbon.[3-9] The Li/Cl_2 cell was operated well above the melting point of LiCl (610°C). At such high temperatures, the electrode reactions are very rapid, and high power densities were achieved (up to 40 W/cm^2). As is to be expected, the corrosion problems were severe. The lifetimes of the Li/Cl_2 cells were short because of flooding of the porous carbon electrode by the LiCl electrolyte, and because of corrosion by the hot Cl_2.

The difficulties of maintaining a stable electrode of liquid lithium and a stable Cl_2 gas electrode led to the development of a solid Li-Al alloy electrode,[10,11] and a high-specific-area carbon-based electrode which stored chlorine in the adsorbed state.[12] These electrodes permitted longer cycle lives to be obtained, but the sacrifice of specific energy was so great as to leave no specific energy advantage over more conventional cells. A detailed review of the work on these lithium/chlorine cells was presented by Cairns and Steunenberg.[2]

The chalcogens, Te, Se, and S, offer an interesting set of liquid reactants for positive electrodes in lithium cells with molten-salt electrolytes. Because Te melts at 450°C, the Li/Te cells were operated at about 475°C. The good electronic conductivity of Te allowed high power densities to be obtained with very simple current collectors,[13,14] as shown in Figure 2.[15] The high cost, high corrosiveness, and high atomic weight of tellurium made it less attractive than selenium, which in turn was less attractive than sulfur as a positive electrode reactant. Voltage-current density curves for all of these lithium/chalcogen cells are shown in Figure 2.[15] The high power densities evident in Figure 2, coupled with high theoretical specific energies (1200 Wh/kg for Li/Se and 2600 Wh/kg for Li/S) make these couples very

attractive.

As a result of efforts to obtain very long cycle lives with lithium/chalcogen cells, it became clear that the transport of soluble chalcogen-containing species[2] from the positive electrode through the electrolyte to the lithium electrode was a major cause of capacity loss. In addition, some difficulty was experienced with the gradual loss of lithium from its current collector. These problems led to the development of solid electrodes comprised of lithium alloys (for negative electrodes) and sulfur compounds (for positive electrodes). Two systems of major current interest are under development using this approach. They are Li-Al/LiCl-KCl/FeS, and Li-Si/LiCl-KCl/FeS_2.

B. The Li-Al/LiCl-KCl/FeS Cell.

The selection of Li-Al as the solid alloy for the negative electrode was the result of a search for an alloy of low weight per equivalent of lithium stored, high transport rates for lithium, low cost, and only modest reduction in cell voltage. The phase diagram for the Li-Al system[16] (Figure 3) shows that aluminum can accept up to about 50 atom percent lithium, with the formation of only a single "compound," LiAl, the β phase in Figure 3. The α + β field of Figure 3 is characterized by an electrode potential of 0.3 V positive with respect to pure Li[17] (E(mV vs. Li^o) = 451.07-0.2202T(^oK)). The broad composition range over which the Li-Al electrode potential remains at 0.3 V is a desirable feature, since it provides for a broad plateau in the discharge curve. The loss of 0.3 V from the cell potential is not very desirable, but is acceptable, considering the fact that a great increase in cycle life is obtained (up to several hundred cycles, compared to perhaps 100 cycles for pure Li). The transport rate of Li in Al and LiAl is sufficient to support superficial current densities of about 100 mA/cm^2 at 450°C.[18]

Iron monosulfide is an inexpensive material that can serve as a positive electrode reactant in a molten lithium halide-containing electrolyte. The iron serves to immobilize the sulfur in a form that has very low solubility in the electrolyte, yet has the capability of being discharged and recharged hundreds of times. The FeS electrode has a potential of about 1.6 V vs. Li, as compared to 2.2-2.3 V vs. Li for S.

The result of immobilizing the Li in LiAl and the S in FeS reduces the theoretical specific energy from 2600 Wh/kg for Li/S to 458 Wh/kg for LiAl/FeS, but provides for a dramatic increase in stability of cell operation and cycle life. The overall cell reaction is:

$$2LiAl + FeS \rightarrow Li_2S + Fe + 2Al \qquad (2)$$

This reaction is a simplification of the process which is better understood by a careful examination of Figure 4.[19-22] The dashed line H-M in Figure 4 is the path followed by the overall composition of the FeS electrode as it is discharged. At point H, the electrode is in the fully charged condition. As lithium is added to the FeS electrode by electrochemical reaction, two new phases are formed, according to the reaction:

$$2FeS + 2Li \rightarrow Li_2FeS_2 + Fe \qquad (3)$$

The emf for this reaction at 450°C is 1.64 V vs. Li.[19] As the overall electrode composition moves into the Li_2S-Fe-E field of Figure 4 as a result of continued discharge, all of the FeS has disappeared, and Li_2S appears:

$$Li_2FeS_2 + 2Li \rightarrow 2Li_2S + Fe \qquad (4)$$

The emf for Reaction 4 at 450°C is 1.62 V vs. Li.[19] When the overall composition of the positive electrode reaches point M of Figure 4, the cell is completely discharged.

Because the potentials for Reactions 3 and 4 are within 25 mV of one another at 450°C,[19] the overall discharge appears to take place at a single potential (1.6 V vs. Li), yielding only one plateau in the voltage vs. capacity plot, as shown in Figure 5.[23]

It has been found that KCl from the LiCl-KCl electrolyte may react with the FeS electrode to form another solid phase in addition to those discussed above. High KCl concentrations, and temperatures below about 500°C favor the formation of djerfischerite ($LiK_6Fe_{24}S_{26}Cl$),[21] which interferes with rapid and complete recharge to FeS.

The complications in the cell chemistry caused by the formation of djerfischerite can be illustrated by the following reactions:

$$6Li + 26FeS + 6KCl \rightarrow LiK_6Fe_{24}S_{26}Cl + 2Fe + 5LiCl \quad (5)$$

$$20Li + LiK_6Fe_{24}S_{26}Cl + 5LiCl \rightarrow 13Li_2FeS_2 + 11Fe + 6KCl \quad (6)$$

$$46Li + LiK_6Fe_{24}S_{26}Cl + 5LiCl \rightarrow 26Li_2S + 24Fe + 6KCl \quad (7)$$

Reaction 5 represents the formation of djerfischerite from the fully-charged FeS electrode as the first step in the discharge process. Next (Reaction 6), djerfischerite reacts to form Li_2FeS_2, or alternatively (Reaction 7) to form Li_2S, depending on temperature (see below).

As is to be expected from Equation 5, the extent of formation of djerfischerite is reduced by lower KCl concentrations in the electrolyte. This is evident from a comparison of Figures 6 and 7.[24] Figure 6 represents the situation with 58.8 m/o LiCl-41.2 m/o KCl (mp = 352°C) as the electrolyte, and Figure 7 corresponds to 66.7 m/o LiCl-33.3 m/o KCl (liquidus temp = 425°C) electrolyte. A more complete discussion of Reactions 3 through 7 and the corresponding thermodynamics can be found in Reference 24.

Figures 6 and 7 also show that djerfischerite can be avoided by operation at higher temperatures, but this increases corrosion rates. Elimination of potassium ion from the electrolyte is another way of avoiding djerfischerite, and the 22 m/o LiF-31 m/o LiCl-47 m/o LiBr (liquidus temp = 430°C) is a candidate electrolyte for this purpose.

Lithium-aluminum/iron monosulfide cells of various sizes and designs have been constructed and tested. A schematic drawing of a cell having a 200 Ah theoretical capacity is shown in Figure 8.[25] The electrodes are comprised of plaques of active material held against metal current collector sheets, and enclosed by metal frames and fine-pored particle retainers welded in place. The plaques of active material are prepared by pressing mixtures of powdered active material (FeS or LiAl) and electrolyte in a mold. Between the electrodes are sheets of separator such as boron nitride felt or powdered MgO held together by electrolyte. Iron and stainless steel are used for the metallic parts of the cell. The electrodes and separators are stacked together as shown in Figure 8, are enclosed by sheets of separator, and are placed in the

cell container. The electrode terminals are welded to bus-bars which are connected to terminals on the cell top. The top is hermetically sealed to the cell container by welding. The positive terminal is a hermetically sealed and insulated feedthrough. A tube attached to the cell top can be used for evacuation and electrolyte addition, as desired, before the cell is finally sealed.

Life-testing of LiAl/FeS cells has disclosed a number of problems which have been the subject of recent cell development efforts. The problems include:

1) Swelling of the electrodes and cells as a result of cycling.

2) Poor wetting of the BN separator.

3) Low specific power.

4) Difficult recharging because of djerfischerite formation.

5) Shorting of the cell due to electrode swelling.

6) Shorting due to extrusion of active material from the positive electrode.

7) Shorting due to protrusions from the LiAl electrode.

8) Capacity loss due to agglomeration of the LiAl.

9) Corrosion of the FeS electrode current collector.

All of the above problems have been eliminated or reduced in severity by various means. Some examples include:

1) Cell swelling eliminated by mechanical restraints.

2) Wetting of the BN separator by electrolyte is improved by depositing MgO on the BN. Also, use of MgO powder separators avoids this wetting problem.

3) Electrode swelling has been reduced by particle retainer screens and perforated sheets. This has also reduced extrusion.

4) Specific power has been increased by improved current collector designs.

5) Djerfischerite formation is reduced by use of LiCl-rich electrolyte, or eliminated by use of an all lithium cation electrolyte.

6) Agglomeration of LiAl is reduced by optimizing the electrolyte content of the electrode.

7) Addition of Fe powder to the FeS electrode reduces the corrosion rate of the Fe current collector.

Some results of the life-testing of LiAl/FeS cells are shown in Figure 9.[26] Statistically meaningful life tests have been performed using groups of twelve identically-constructed cells for each test group. Recent results show that cells of 150 Ah and 350 Ah capacities have a mean cycle life to failure of 300-450 deep cycles (100% depth of discharge), with some cells exceeding 1000 cycles. The capacity loss was 0.025-0.06 percent per cycle. Failure was defined as 20% loss of capacity, or a coulombic efficiency below 95%. These cells had a specific energy of 80-95 Wh/kg, and a peak specific power of 70-80 W/kg. Recent cells designed for high specific power yielded about 90 Wh/kg and up to 135 W/kg at 50% state of charge.[23]

Thermal cycling of cells between ambient temperature and operating temperature (450-475°C) was originally detrimental to cell performance, but improvements in cell construction have resulted in cells that can be thermally cycled between ambient temperature and operating temperature more than sixty times without detectable capacity loss.[23] This improvement is largely traceable to the use of a very effective wetting agent (MgO deposit) on the BN felt separator.

A small number of ten-cell batteries of LiAl/FeS cells have been tested.[23,25,27] These batteries were comprised of 350 Ah cells, and had an energy storage capability of 4 kWh (measured at 70 A). The cycle lives of the batteries were 150 to 275 cycles. The charge and discharge curves for one of these batteries at cycle number 250 are shown in Figure 10. Typical watt-hour efficiencies of 80-85 percent were achieved.

Thermal control of these batteries requires a knowledge of the heat generation rate during various conditions of operation. Of course, the heat generation rate is comprised of the reversible heat generation rate and the irreversible heat generation rate:

$$\dot{Q} = I \left[-T\left(\frac{\partial E}{\partial T}\right)_{P,\xi} + \eta \right] \qquad (8)$$

where $\dot{Q}$ = heat generation rate, watts

I = current, amperes

T = temperature, ^{o}K

E = reversible cell potential, volts

P = pressure

ξ = extent of cell reaction

η = overvoltage, volts

Figure 7 shows that $\left(\frac{\partial E}{\partial T}\right)$ varies from negative to positive to negative as the discharge proceeds at 475°C. Of course, the product $I\eta$ is always positive. It is thus possible to have $\dot{Q}$ either positive or negative depending on the relative values of $IT\left(\frac{\partial E}{\partial T}\right)$ and $I\eta$. This is shown to be the case in Figure 11,[28] for a 200 Ah cell at various discharge currents, operating at 475°C.

No thermally self-sustaining and automatically controlled LiAl/FeS batteries have yet been operated, but low-thermal-conductivity enclosures have been developed, and one of the next stages in battery development would include such operation.

The lithium-aluminum/iron monosulfide system is in the most advanced state of development of any rechargeable molten-salt battery. It has shown good stability, ruggedness, and ability to be thermally cycled. It may find application for stationary energy storage, and possibly in electric vehicles.

C. The Li-Si/LiCl-KCl/FeS_2 Cell.

The Li-Si electrode accomplishes the same purpose of immobilizing lithium as the Li-Al electrode, but the Li_4Si electrode reactant weighs only 0.52 g/Ah, as compared to 1.27 g/Ah for LiAl. This represents a significant weight saving for the cell. In addition, FeS_2 weighs only 1.12 g/Ah, compared to 1.64 g/Ah for FeS. These weight savings, combined with the higher cell voltage attributable to FeS_2 raise the theoretical specific energy to 944 Wh/kg for the overall cell reaction:

$$Li_4Si + FeS_2 \rightarrow 2Li_2S + Fe + Si \qquad (9)$$

A theoretical specific energy of 944 Wh/kg permits the development of a complete cell with a specific energy of about 200 W-h/kg (see below).

The Li-Si electrode is governed by a relatively complex phase diagram, as shown in Figure 12.[29] Some more recent work[30] argues for slightly more silicon-rich compositions for the compounds indicated in Figure 12. Four voltage plateaus are encountered in the discharge of the Li_4Si electrode, in keeping with the phase diagram. At 450°C, these are:[30]

$Li_{3.9}Si \rightarrow Li_{3.25}Si$	42 mV vs. Li
$Li_{3.25}Si \rightarrow Li_{2.33}Si$	150
$Li_{2.33}Si \rightarrow Li_{1.71}Si$	277
$Li_{1.71}Si \rightarrow Si$	326

Note that these potentials are similar to (and on the average, somewhat lower than) those of the Li-Al electrode.

The FeS_2 electrode is just as complex as the FeS electrode, as can be seen from Figure 4. The path followed by the FeS_2 electrode during its discharge is indicated by the line AFEL in Figure 4. There are four stages in the overall process:[30]

$$2FeS_2 + 3Li \rightarrow Li_3Fe_2S_4 \qquad E = 2.04\ V \qquad (10)$$

$$Li_3Fe_2S_4 + Li \rightarrow Fe_{1-x}S + Li_{2+x}Fe_{1-x}S_2 \qquad E = 1.9\ V \qquad (11)$$

$$Fe_{1-x}S + Li_{2+x}Fe_{1-x}S_2 + Li \rightarrow Li_2FeS_2 \qquad E = 1.9\text{-}1.62\ V \qquad (12)$$

$$2Li_2FeS_2 + 4Li \rightarrow 4Li_2S + 2Fe \qquad E = 1.62\ V \qquad (13)$$

The potential of Reaction 10 is reported as being insensitive to extent of reaction, a condition that is inconsistent with only two phases (FeS_2 and $Li_3Fe_2S_4$) being present. One explanation for this observation of constant potential would be that the FeS_2 loses some sulfur by vaporization, yielding some $Fe_{1-x}S$, which then would stabilize the electrode potential, providing the required third phase. This argument is supported by the observation that in a fully-charged FeS_2 electrode, some $Fe_{1-x}S$ is present.[30]

Reaction 11 involves three phases in the positive electrode, and should therefore have a stable potential. Reaction 11 is not balanced, and involves only about 4.3% of the coulombs that correspond to Reactions 10 through 13 (see Figure 4). Reaction 12 is also unbalanced, involves only two phases in

the positive electrode ($Fe_{1-x}S$ and $Li_{2+x}Fe_{1-x}S_2$), and therefore should not have a constant potential. This is indeed the observation--a potential that declines with state of charge from 1.9 to 1.62 V vs. Li, over a narrow composition range corresponding to 8.2% of the total discharge.

The final stage of the discharge reaction for the FeS_2 electrode is the conversion of Li_2FeS_2 to Li_2S and Fe; which occurs at a potential of 1.62 V vs. Li at 450°C. Figure 13 shows a discharge curve for an FeS_2 electrode at 417°C and 12 mA/cm^2. The LiAl reference electrode is 300 mV positive to Li.

The presence of high concentrations of KCl in the electrolyte can cause the formation of minor amounts of djerfischerite and $KFeS_2$, but these compounds have not interfered with the operation of the cell, in contrast to the case for the FeS electrode. Experiments with various LiCl concentrations in the LiCl-KCl electrolyte have shown higher utilizations of FeS_2 at the higher LiCl concentrations (68 m/o LiCl).[31]

The state of development of engineering-scale hardware for the Li-Si/FeS_2 cell is not as mature as for the Li-Al/FeS cell. Almost all of the results reported have been for single cells of less than 100 Ah capacity. A typical disk-shaped Li-Si/FeS_2 cell is shown in Figure 14.[32] This type of cell has a central, disk-shaped positive electrode made of a pressed mixture of powdered FeS_2, electrolyte, and graphite powder current collector. Molybdenum mesh is also used as a current collector, and is attached to a central molybdenum rod which is part of a vacuum-tight feedthrough. Zirconia cloth is placed around the positive electrode to act as a particle retainer and separator. Boron nitride cloth (or felt) is used as a second separator layer. On each side of the positive electrode-separator assembly is a negative electrode comprised of Li-Si powder in a current collector such as reticulated nickel. The negative electrodes are kept in electronic contact with the stainless-steel cell container, which also serves as the negative terminal. Typically, the cells are about 13 cm dia and have a capacity near 70 Ah.[32]

The charge and discharge curves for Li-Si/FeS_2 cells have two major plateaus, as is to be expected on the basis of Equations 10-13, and Figure 13. Cells like those of Figure 14 have yielded the performance data shown in Figure 15.[32] The weight used in calculating the specific power and specific energy values of Figure 15 did not include any insulation weight, but was the

full weight of the cell as shown in Figure 14. Notice that specific energy values as high as 185 Wh/kg (20% of theoretical) were achieved, albeit at low specific power. Also, specific power values as high as about 100 W/kg were achieved. With improved cell design, it is to be expected that specific energies in excess of 200 Wh/kg will be obtained, at specific powers of 30-35 W/kg, and specific powers of at least 150 W/kg will be achieved.

Life-testing of Li-Al/FeS_2 and Li-Si/FeS_2 cells has resulted in the data shown in Figure 16.[32] These cells are capable of operating for at least 700 cycles and 15,000 hours. Experience with these cells has resulted in the identification of a number of problems that require attention before practical systems can be developed. These problems include:

1. Swelling of the positive electrodes as a result of cycling.
2. Poor wetting of the BN separator.
3. Specific power lower than desired.
4. Cell shorting due to swelling and extrusion of positive active material.
5. Capacity loss due to loss of sulfur from the positive electrode.
6. Corrosion of the current collectors, especially in the positive electrode.

Recent progress has been made on some of these problems. The BN wetting problem is reduced by the use of an MgO deposit on the BN surface. Improved containment of the positive active material reduces electrode swelling, extrusion, and shorting. Sulfur loss rates are reduced by careful control of recharge conditions, avoiding high sulfur activities.[33] Molybdenum may have an acceptably low corrosion rate in the FeS_2 electrode, but it is unclear that economic considerations will allow the use of adequate amounts of molybdenum.

The experience with Li-Al/FeS_2 and Li-Si/FeS_2 batteries is very limited. Some small bipolar two-cell batteries have been operated,[34] and have lasted several hundred cycles and up to 11,000 hours. More experience is needed with larger cells (at least 100 Ah), and batteries (more than 10 cells) before the full range of systems engineering problems can be addressed.

Figures 15 and 16, and other data show that Li-Si/FeS_2 cells having a specific energy of about 200 Wh/kg can be operated for about 700 cycles and two years. Scale up to larger cell sizes and experience with batteries are needed. Corrosion problems at the positive electrode, and sulfur loss problems must be addressed more thoroughly.

D. Lithium Cells with Molten Nitrate Electrolytes.

Molten alkali nitrate mixtures offer the attractive possibility of having molten-salt cells that operate at 100-200°C instead of 350-500°C. Recent work[35] has shown that solid lithium in contact with a $LiNO_3$-KNO_3 eutectic electrolyte (41 m/o $LiNO_3$) at 150°C forms a thin (10-100 Å) film of Li_2O which protects the lithium from rapid attack by the electrolyte. The film dissolves (and is regenerated) at a rate of 10-100 $\mu A/cm^2$ at 150°C, so the self-discharge of the lithium electrode may be tolerable. (Complete self-discharge for a typical capacity density of 0.3 A-h/cm^2 would require at least 3000 h.)

Care must be taken in selecting positive electrodes for use in the strongly-oxidizing nitrate electrolyte. The positive electrode reactant must therefore resist oxidation, and be capable of reacting reversibly with lithium ions from the electrolyte. It has been found that V_2O_5 can accept one lithium atom per V_2O_5,[35] and that the reaction is reversible:

$$Li + V_2O_5 \rightleftharpoons LiV_2O_5 \qquad (14)$$

The potential of this reaction covers a range from 3.6 to about 3.5 volts vs. Li. Simple small laboratory cells have been cycled at the 3-4 hour rate. Other positive electrode reactants may also be used, but they must be operated within the potential range 2.9-3.5 V vs. Li, which is the range of stability of the nitrate electrolyte. Below 2.9 V, nitrate is reduced to nitrite and oxide ions; above 3.5 V, the nitrite produced at the Li electrode is oxidized to NO_2 gas.

There is also a narrow temperature range within which the solid lithium/molten $LiNO_3$-KNO_3 half cell can be safely operated. The electrolyte melts at 135°C, and lithium melts at 180°C. Above 180°C, there is danger of rupture of the Li_2O film, and explosive reaction between Li and NO_3^-. It may be possible to extend the operating temperature range by the use of solid lithium alloys such as Li-Al or Li-Si.

It is too early to evaluate the possibilities of developing practical rechargeable cells based on lithium negative electrodes and molten nitrate electrolytes.

III. Lithium Cells with Solid Electrolytes

The search for solid electrolytes that conduct lithium ions and are stable in contact with elemental lithium has been disappointing so far. A large number of lithium-containing compounds and mixtures of compounds, in both crystalline and glassy forms have been evaluated for lithium-ion conductivity and stability in contact with lithium. All of the materials tested have either shown low conductivity or instability to lithium, or both. As an example, the lithium form of beta alumina ($Na_2O \cdot 11Al_2O_3$) has only one tenth the ionic conductivity that the sodium form has, and it is unstable in contact with lithium. Lithium halides are stable in contact with lithium, and do have a modest lithium ion conductivity, which increases with increasing temperature, as shown in Figure 17.[36] It has been found that mixtures of lithium iodide and high-area alumina have a lithium-ion conductivity much higher than LiI alone. This mixture has been used in $Li_4Si/LiI\text{-}Al_2O_3/TiS_2$ cells, as described below.

A. The $Li_4Si/LiI\text{-}Al_2O_3/TiS_2$ Cell.

This cell represents an all-solid-state cell, even at its elevated operating temperature of 300-325°C.[37] The negative electrode is the same as the one discussed above in connection with the Li-Si/FeS_2 cell. The positive electrode is powdered TiS_2 pressed into a titanium mesh current collector. The TiS_2 is a layered compound having the capability of reversibly intercalating up to one Li atom per Ti atom, without destroying the basic layered structure of TiS_2.[38] The overall reaction is:

$$\tfrac{1}{4}\,Li_4Si + TiS_2 \rightarrow LiTiS_2 + \tfrac{1}{4}\,Si \qquad (15)$$

The theoretical specific energy for this cell reaction is 415 Wh/kg.

Cells can be prepared by pressing layered pellets of powdered Li_4Si plus powdered electrolyte into a Ti current collector as the negative electrode, pressure-bonded to a layer of $LiI\text{-}Al_2O_3$ electrolyte, which in turn is bonded to the TiS_2-Ti mesh positive electrode.[37] The total thickness is about 3

mm, and the diameter about 3 cm. Cells of this type having a capacity of 0.4 Ah and an average discharge voltage of about 1.75 V have been operated at 300-325°C at current densities of 5-10 mA/cm^2 for almost 500 cycles with good coulombic efficiencies, but relatively low utilizations, as shown in Figure 18.

Problems encountered with the Li_4Si/TiS_2 all-solid cell include low utilization of the active materials, low current densities, and high internal resistance. Higher-conductivity electrolytes would reduce these problems. It is too early to determine if cells of this general type will have performance adequate for use in large batteries as for electric vehicles or stationary energy storage.

IV. Future Directions

The material presented in this chapter provides incentive for continued research and development of high-temperature lithium batteries, because they have already demonstrated significantly higher specific energies than are available from any other rechargeable batteries. In addition, cycle lives of several hundred to over one thousand deep cycles have been reported. This combination of high performance and long life, when coupled with low potential cost, offers the possibility of widespread use in highly-demanding applications, including electric vehicles, stationary energy storage, and aerospace power. Before these applications can be realized, progress is needed in a number of areas, including:

- Corrosion-resistant current collectors for high-sulfur-activity electrodes.
- Improved containment of electrode reactants in the electrode structures.
- Lower-cost separators.
- High-conductivity, stable lithium-ion conducting solid electrolytes.
- Reliable vacuum-tight feedthroughs that are corrosion-resistant.

REFERENCES

1. E.J. Cairns, in Comprehensive Treatise of Electrochemistry, Vol. 3, J.O'M. Bockris, B.E. Conway, E. Yeager, and R.E. White, eds., Plenum Publishing Corporation, New York, 1981, p. 341.

2. E.J. Cairns and R.K. Steunenberg, in Progress in High Temperature Physics and Chemistry, Vol. 5, C.A. Rouse, ed., Pergamon Press, New York, 1973, p. 63.

3. D.A.J. Swinkels, J. Electrochem. Soc., 113, 6 (1966).

4. D.A.J. Swinkels, Electrochem. Tech., 5, 327 (1967).

5. D.A.J. Swinkels, J. Electrochem. Soc., 114, 812 (1967).

6. D.A.J. Swinkels, Electrochem. Tech., 5, 396 (1967).

7. D.A.J. Swinkels and S.B. Tricklebank, Electrochem. Tech., 5, 327 (1967).

8. D.A.J. Swinkels and R.N. Seefurth, J. Electrochem. Soc., 115, 994 (1968).

9. D.A.J. Swinkels, IEEE Spectrum, 5, 71 (1968).

10. E.S. Buzzelli, presented to the Southern California-Nevada Section of The Electrochemical Society, Los Angeles, December, 1967.

11. E.S. Buzzelli, U.S. Patent No. 3,445,288, May 20, 1969.

12. J.E. Metcalfe, E.J. Chaney, and R.A. Rightmire, in Proceedings of the 1971 Intersociety Energy Conversion Engineering Conference, Society of Automotive Engineers, Inc., New York, 1971, p. 685.

13. H. Shimotake, G.L. Rogers, and E.J. Cairns, presented at The Electrochemical Society Meeting, Chicago, October, 1967; see also, Extended Abstracts of the Battery Division, 12, 42 (1967).

14. H. Shimotake, G.L. Rogers, and E.J. Cairns, I&EC Process Design and Development, 8, 51 (1969).

15. E.J. Cairns, R.K. Steunenberg, and H. Shimotake, in Kirk-Othmer Encyclopedia of Chemical Technology, Supplement Volume, 2nd edition, H. Standen, ed., John Wiley & Sons, Inc., New York, 1971.

16. K.M. Myles, F.C. Mrazek, J.A. Smaga, and J.L. Settle, in Proceedings of the Symposium and Workshop on Advanced Battery Research and Design, March 22-24, 1976, Argonne National Laboratory Report ANL-76-8 (1976), p. B-69.

17. N.P. Yao, L. Heredy, and R.C. Saunders, J. Electrochem. Soc., 118, 1039 (1971).

18. H. Shimotake, W.J. Walsh, E.S. Carr, and L.G. Bartholme, in Proceedings of the 11th Intersociety Energy Conversion Engineering Conference, Vol. 1, American Institute of Chemical Engineers, New York, 1976, p. 473.

19. Z. Tomczuk, M.F. Roche, and D.R. Vissers, J. Electrochem. Soc., 128, 2255 (1981).

20. A.E. Martin, in High-Performance Batteries for Electric Vehicle Propulsion and Stationary Energy Storage, Argonne National Laboratory Report ANL-78-94 (1978), p. 167.

21. A.E. Martin and Z. Tomczuk, in High Performance Batteries for Electric Vehicle Propulsion and Stationary Energy Storage, Argonne National Laboratory Report ANL-79-39 (1979), pp. 71-73.

22. Z. Tomczuk, M.F. Roche, and D.R. Vissers, presented at The Electrochemical Society Meeting, Hollywood, FL, October, 1980, Abstract No. 78.

23. T.D. Kaun and D.J. Kilsdonk, in Lithium/Iron Sulfide Batteries for Electric-Vehicle Propulsion and Other Applications, Progress Report for October 1979-September 1980, Argonne National Laboratory Report ANL-80-128 (1981), p. 156.

24. Z. Tomczuk, S.K. Preto, and M.F. Roche, J. Electrochem. Soc., 128, 760 (1981).

25. Argonne National Laboratory, Lithium/Iron Sulfide Batteries for Electric-Vehicle Propulsion and Other Applications, Progress Report for October 1980-September 1981, ANL-81-65 (February, 1982).

26. Argonne National Laboratory, Annual DOE Review of the Lithium/Metal Sulfide Battery Program, June, 1979.

27. W.E. Miller, E.C. Gay, and D. Kilsdonk, in Proceedings of the 17th Intersociety Energy Conversion Engineering Conference, Institute of Electrical and Electronic Engineers, New York, 1982, p. 585.

28. H.F. Gibbard, D.M. Chen, C.C. Chen, and T.W. Olszanski, in Proceedings of the 16th Intersociety Energy Conversion Engineering Conference, American Society of Mechanical Engineers, New York, 1981, p. 752.

29. R.A. Sharma and R.N. Seefurth, J. Electrochem. Soc., 123, 1763 (1976).

30. Z. Tomczuk, B. Tani, N.C. Otto, M.F. Roche, and D.R. Vissers, J. Electrochem. Soc., 129, 925 (1982).

31. J.S. Dunning, R.N. Seefurth, and R.A. Murie, presented at The Electrochemical Society Meeting, Hollywood, FL, October, 1980, Abstract No. 77.

32. E.J. Zeitner and J.S. Dunning, in Proceedings of the 13th Intersociety Energy Conversion Engineering Conference, Society of Automotive Engineers, Warrendale, PA, 1978, p. 697.

33. S.K. Preto, Z. Tomczuk, S. von Winbush, and M.F. Roche, J. Electrochem. Soc., in press.

34. T.G. Bradley, in Proceedings of the 15th Intersociety Energy Conversion Engineering Conference, American Institute of Aeronautics and Astronautics, New York, 1980, p. 228.

35. J. Poris, I.D. Raistrick, and R.A. Huggins, in Proceedings of the Symposium on Lithium Batteries, The Electrochemical Society, Pennington, NJ, 1981, p. 459.

36. W. Weppner, in Solid State Ionics, Vol. 5, M.S. Whittingham, et al, ed., North-Holland Publishing Company, Amsterdam, 1981, p. 3.

37. J.R. Rea, G.S. Kelsey, and M. Kallianidis, in Proceedings of the 16th Intersociety Energy Conversion Engineering Conference, American Society of Mechanical Engineers, New York, 1981, p. 761.

38. M.S. Whittingham, J. Electrochem. Soc., 123, 315 (1976).

This work was supported by the U.S. Department of Energy under Contract DE-AC03-76SF00098.

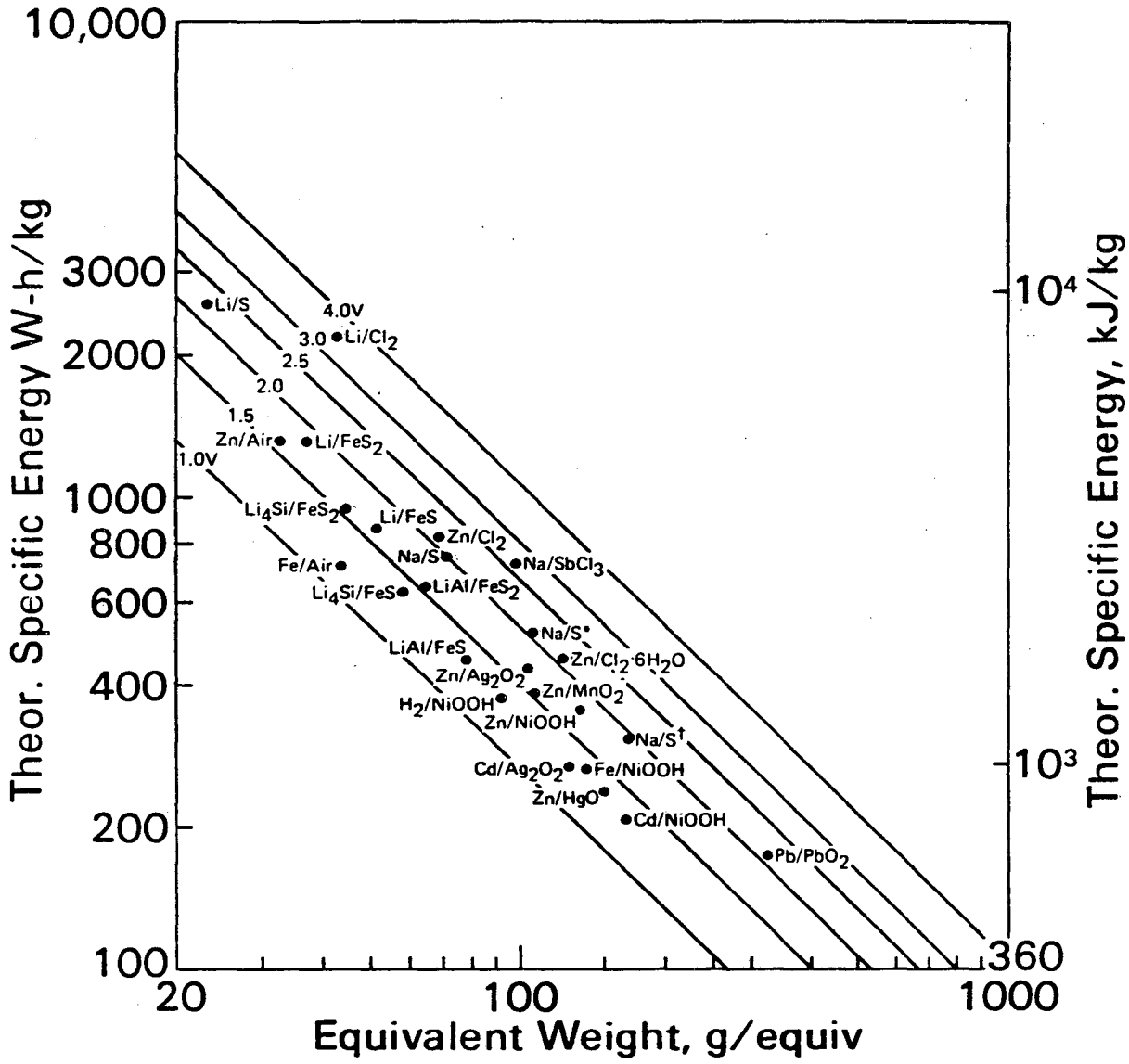

XBL 7912-13725

Figure 1. Theoretical specific energy of candidate cells. Lines are for cell voltages from 1V to 4V, as labeled.

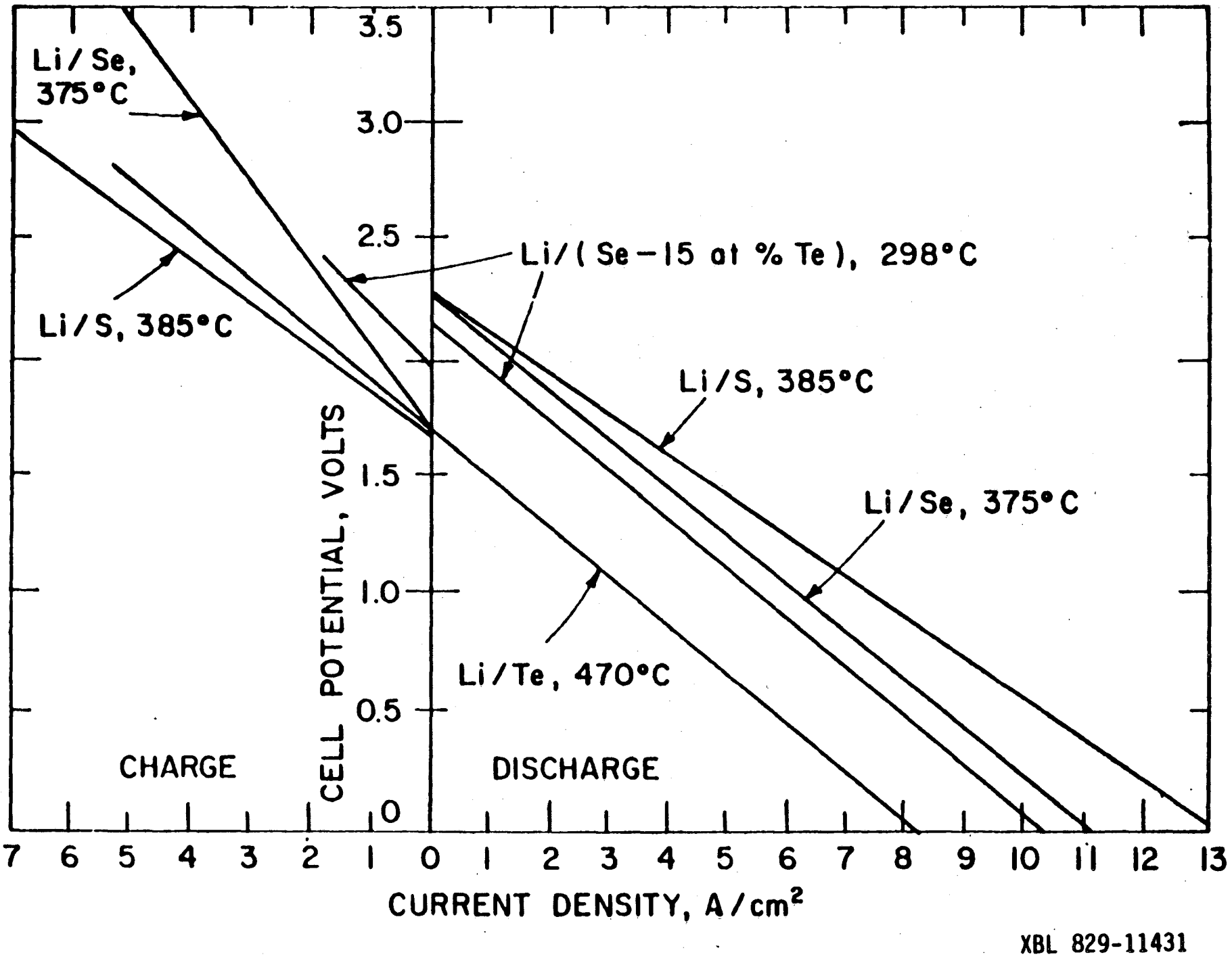

Figure 2. Voltage-current density curves for liquid-electrolyte lithium/chalcogen cells.

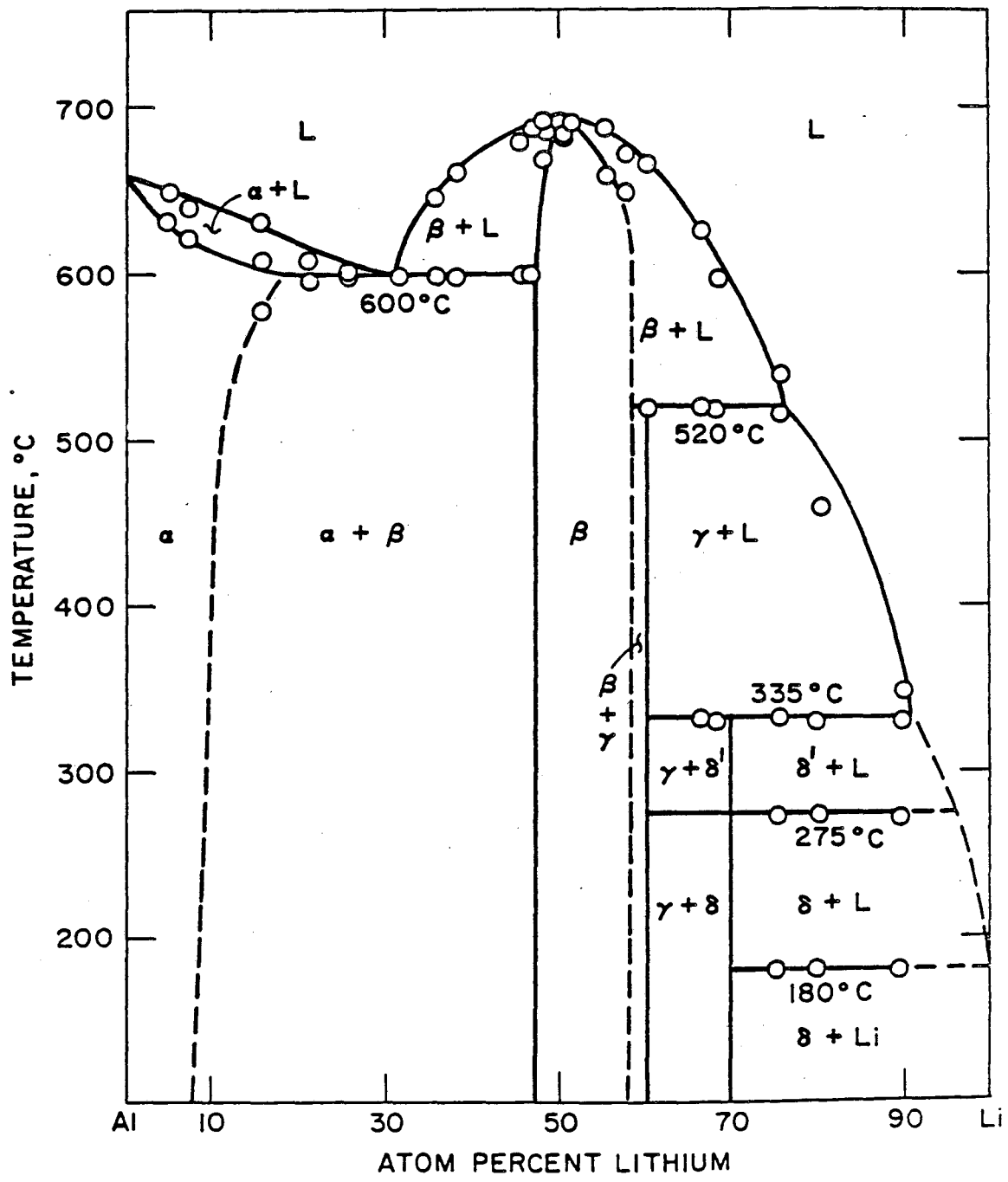

(α = Al, β = LiAl, γ = Li_3Al_2, δ = δ' = Li_9Al_4)

XBL 801-7726

Figure 3. The lithium-aluminum phase diagram.[16]

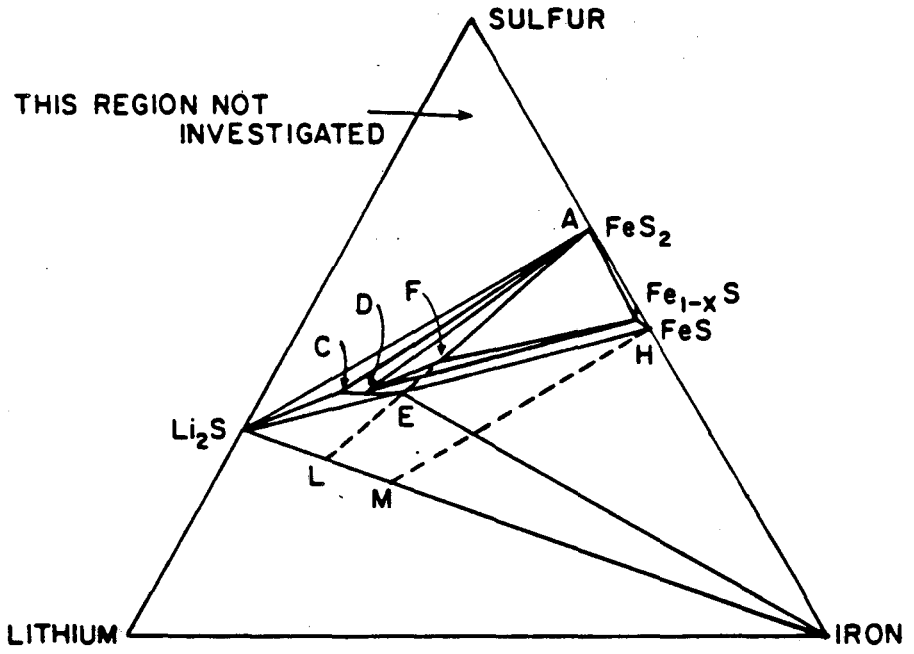

Figure 4. Isothermal section of the Li-Fe-S phase diagram at 450°C.

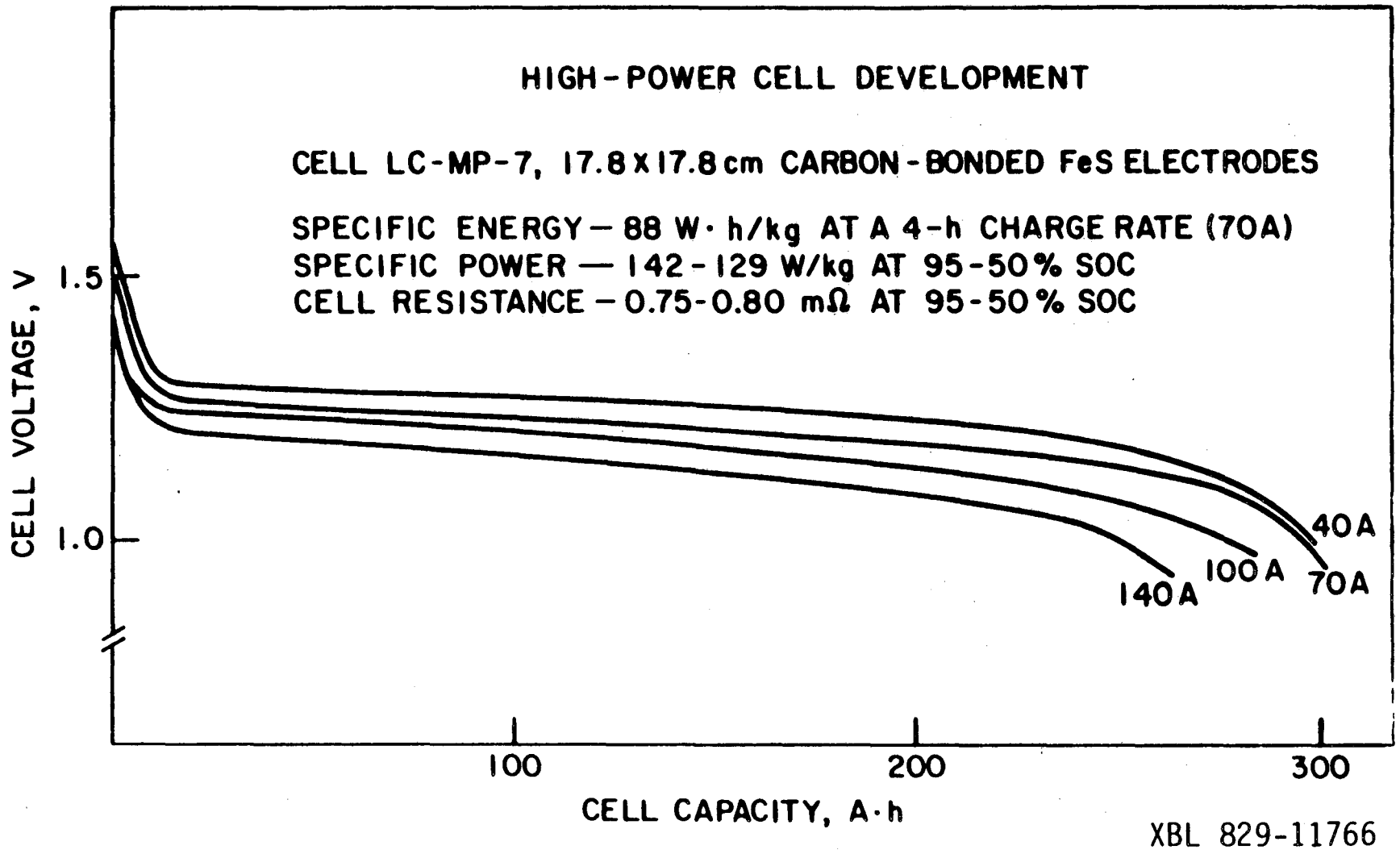

Figure 5. Cell LC-MP-7 (350 A·h Theoretical Capacity) Discharged with Constant Current.

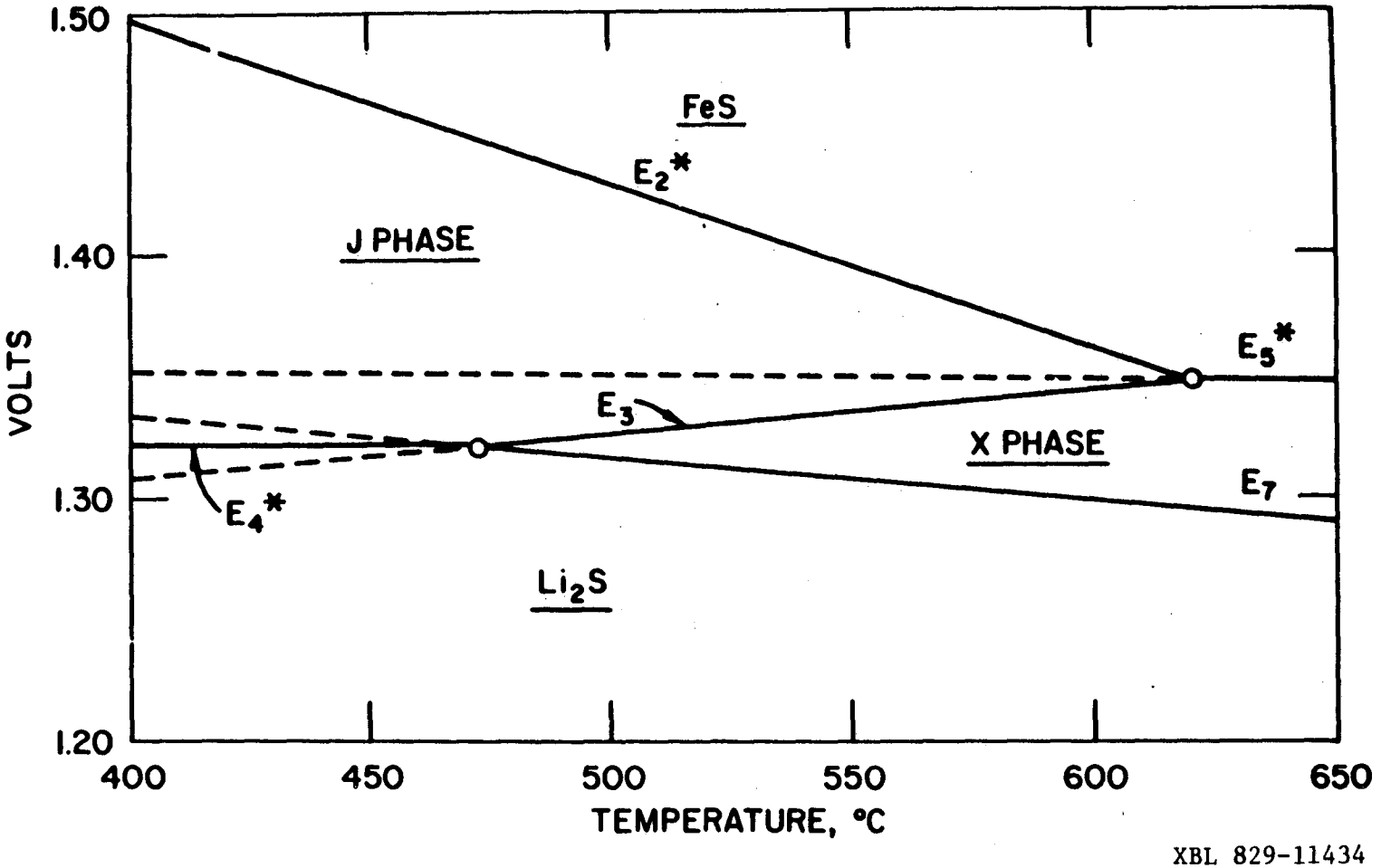

XBL 829-11434

Figure 6. Regions of stability of FeS, djerfischerite (J-phase), Li_2FeS_2 (X-phase), and Li_2S in LiCl-KCl electrolyte of eutectic composition. Extensions of the FeS ↔ X(E_5*), J ↔ X(E_3), and X ↔ Li_2S(E_7) reactions into the low temperature region are indicated by dashed lines. An asterisk indicates a calculated emf.

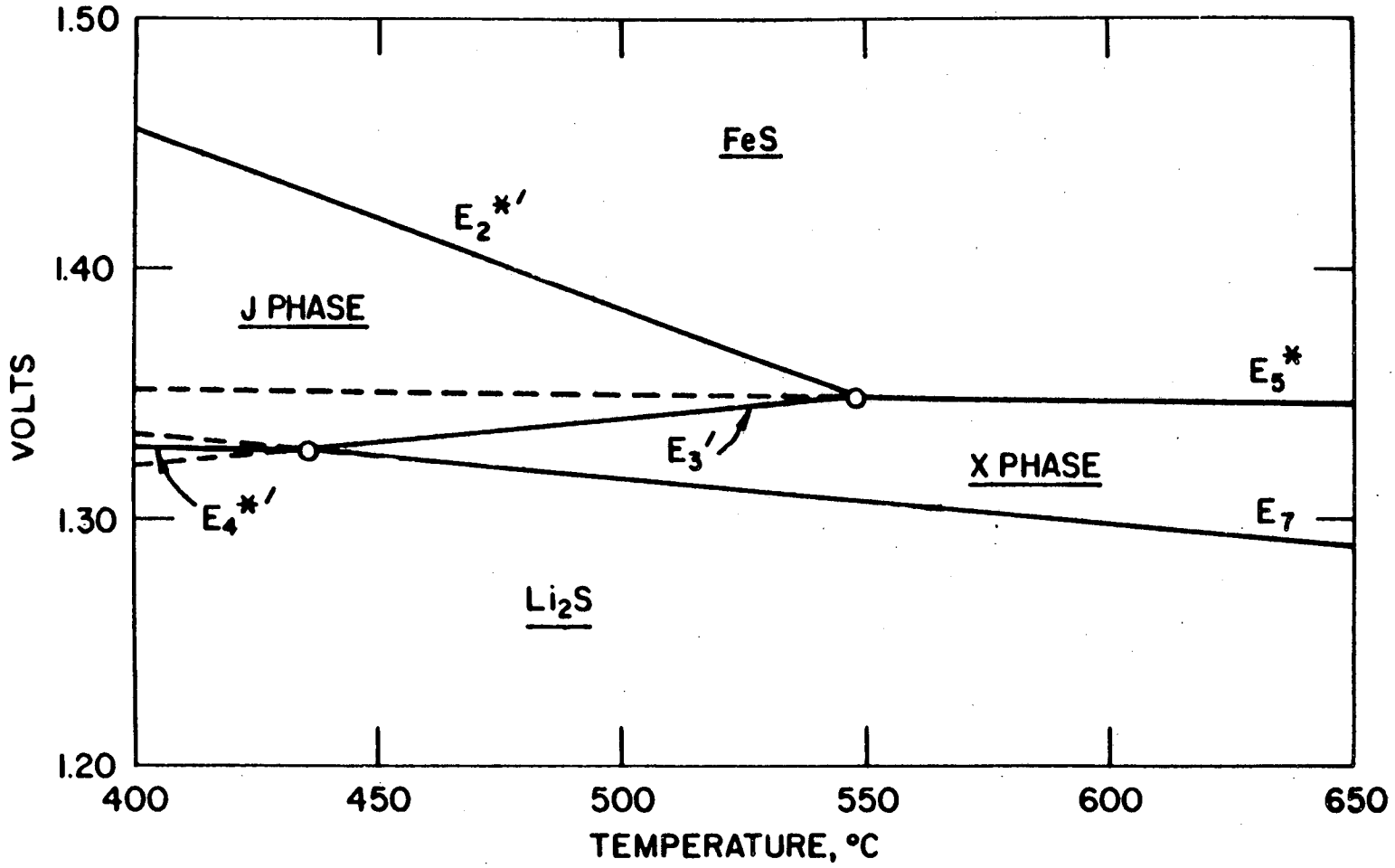

XBL 829-11435

Figure 7. Regions of stability of FeS, J-phase, X-phase, and Li_2S in LiCl-rich electrolyte (67 m/o LiCl). Extensions of the FeS $\leftrightarrow$ X(E_5*), J $\leftrightarrow$ X(E_3'), and X $\leftrightarrow$ Li_2S(E_7) reactions into the low temperature region are indicated by dashed lines. An asterisk indicates a calculated emf. Note that E_2*', E_3', and E_4*' are shifted from their corresponding values in eutectic electrolyte (E_2*, E_3, E_4*), and the field of J-phase stability is therefore much smaller.

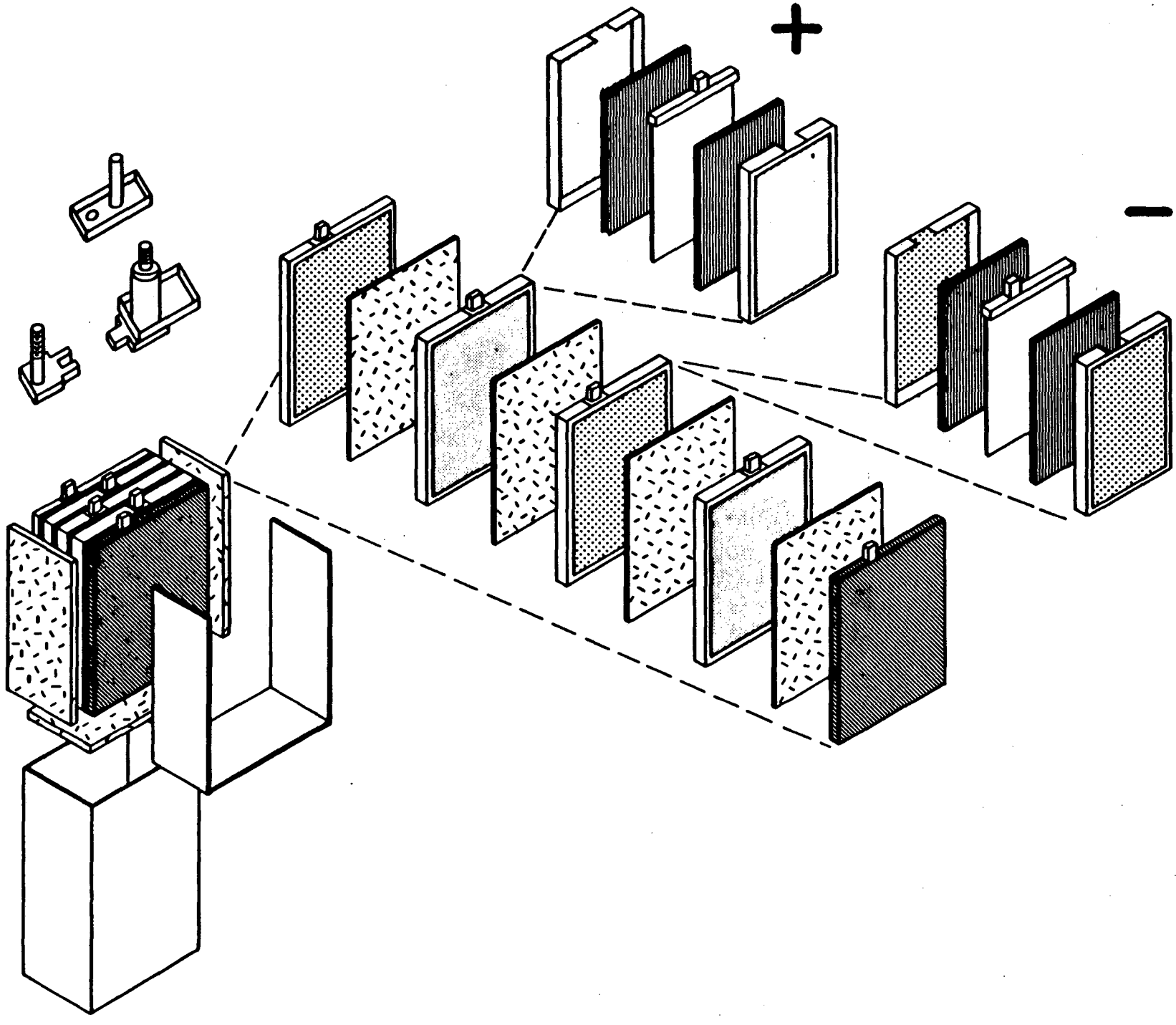

Figure 8. Design Used for the Immobilized Electrolyte/Powder Separator Cells.

XBL 829-11432

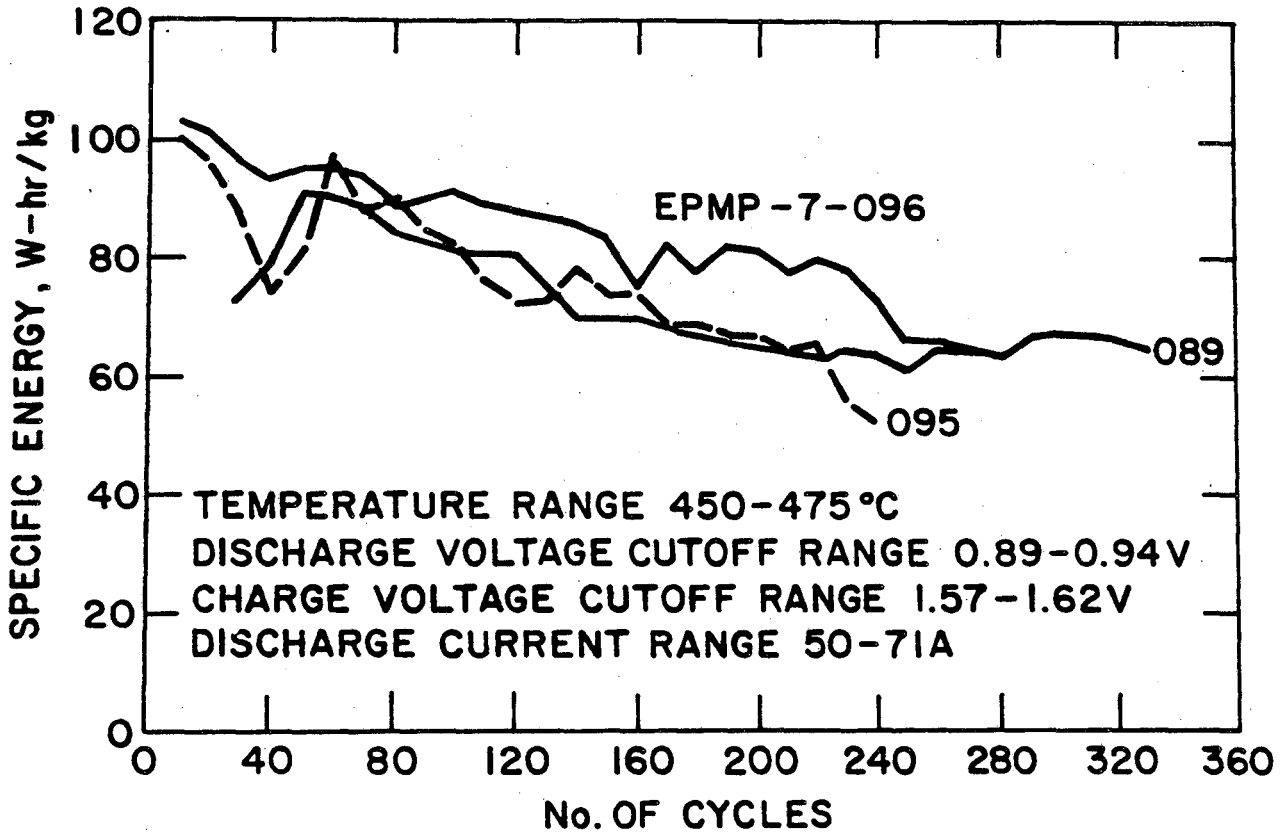

XBL 801-7729

Figure 9. Specific energy vs. cycle number for 300Ah LiAl-FeS cells.

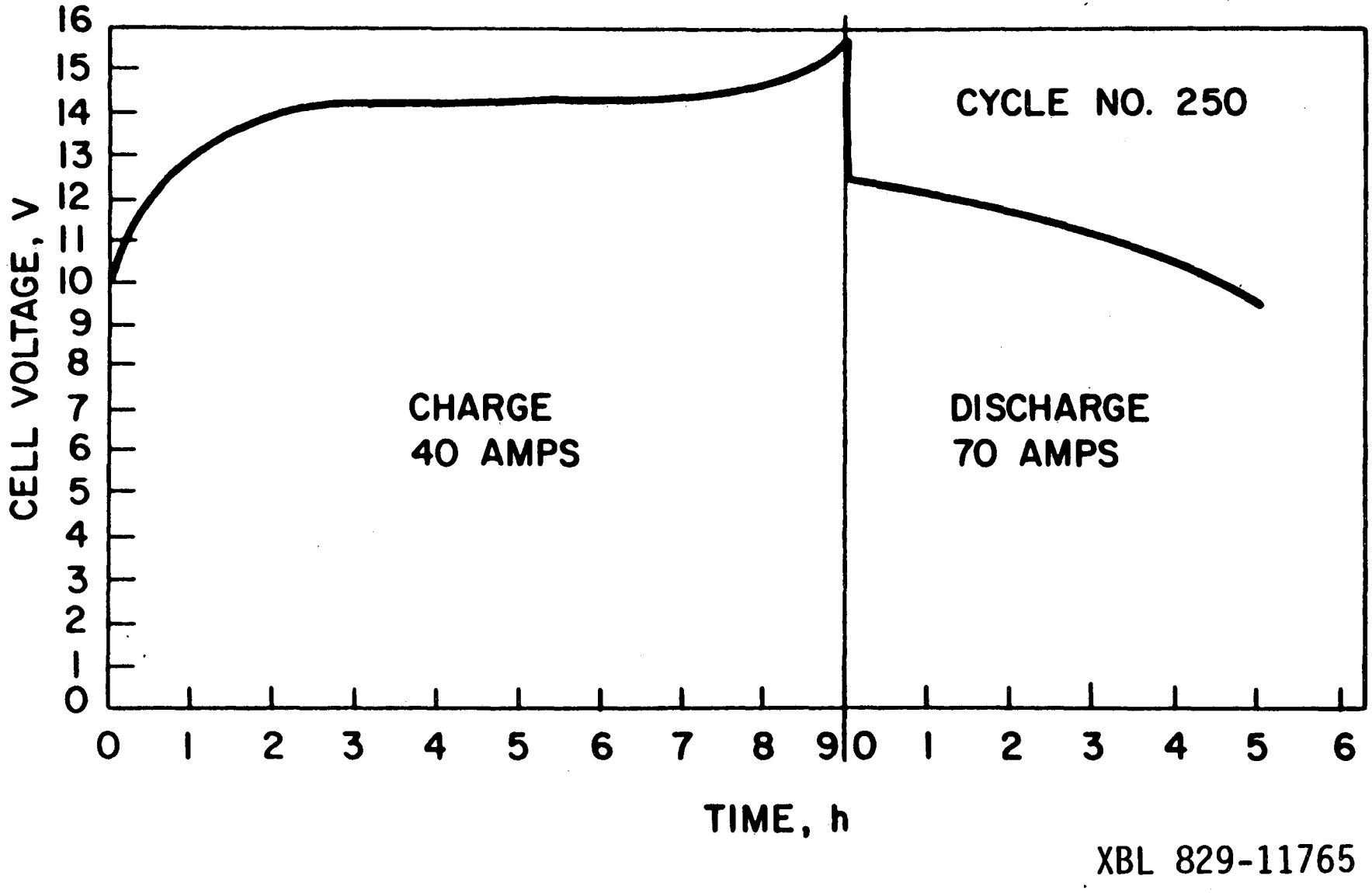

Figure 10. Performance Curve for 10-cell LiAl/FeS Module at Cycle 250.

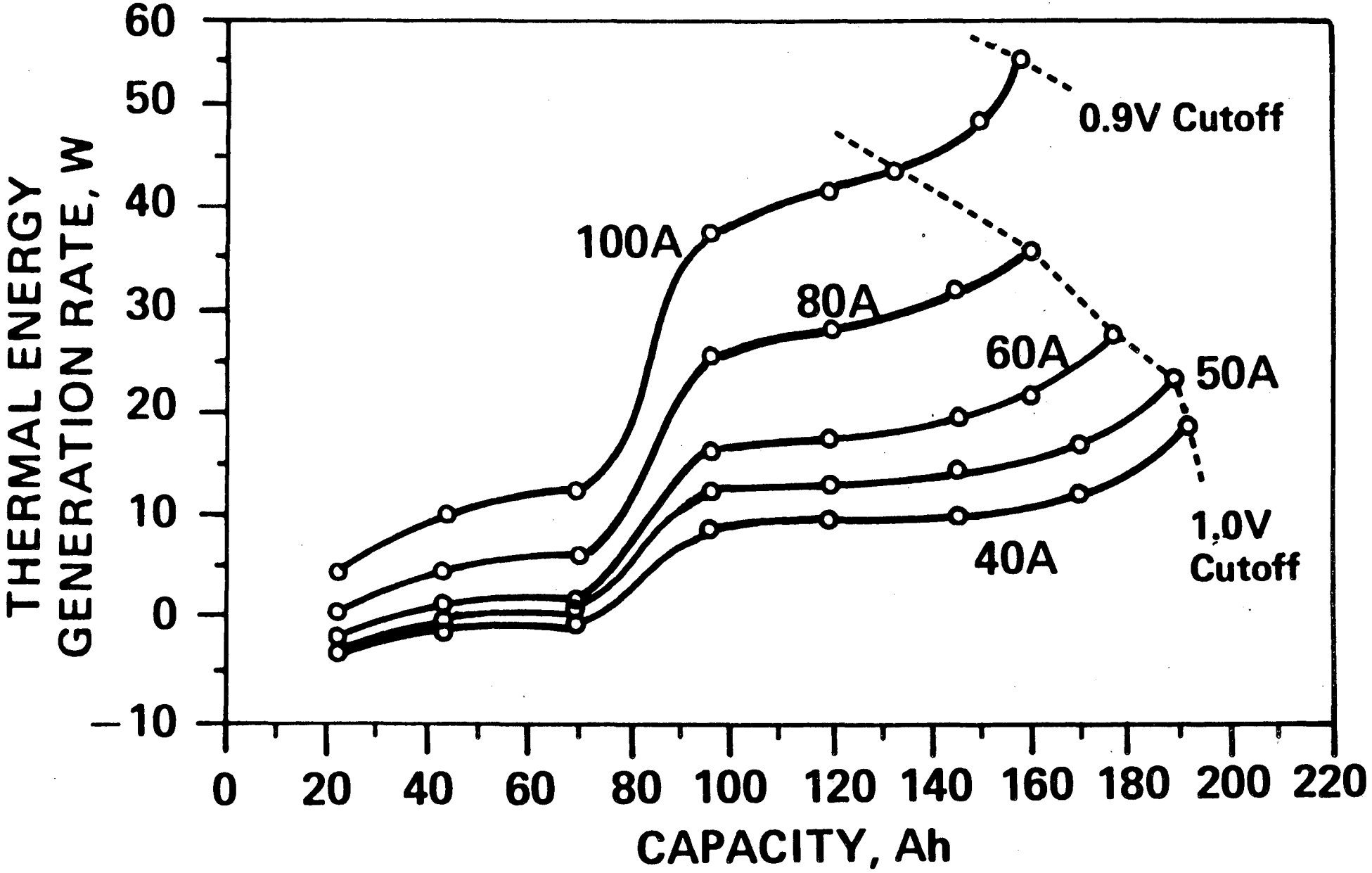

XBL 829-11433

Figure 11. Thermal Energy Generation Rate of a LiAl/FeS Cell at Various Discharge Currents at 475°C.

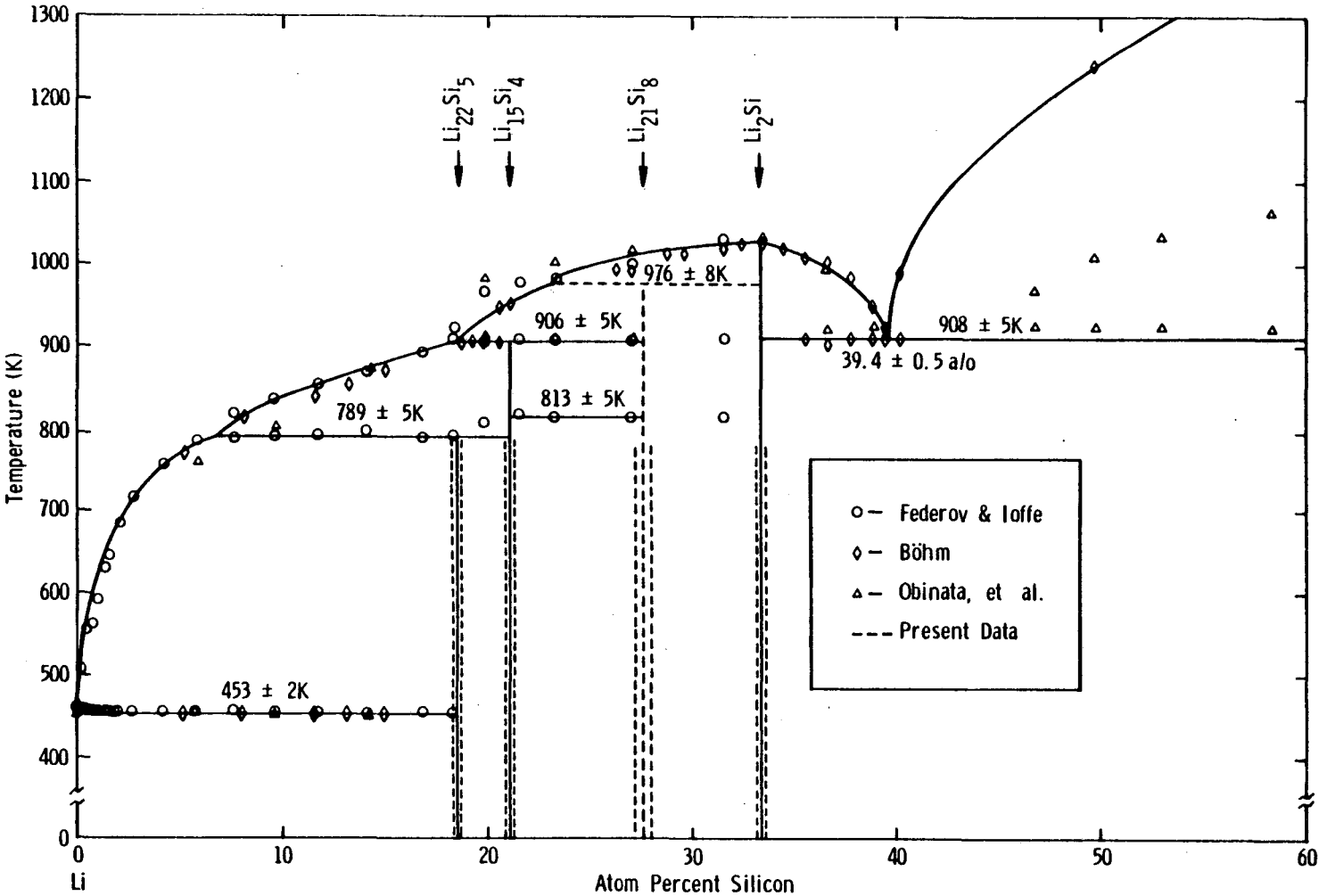

XBL 801-7727

Figure 12. The lithium-silicon phase diagram. (29)

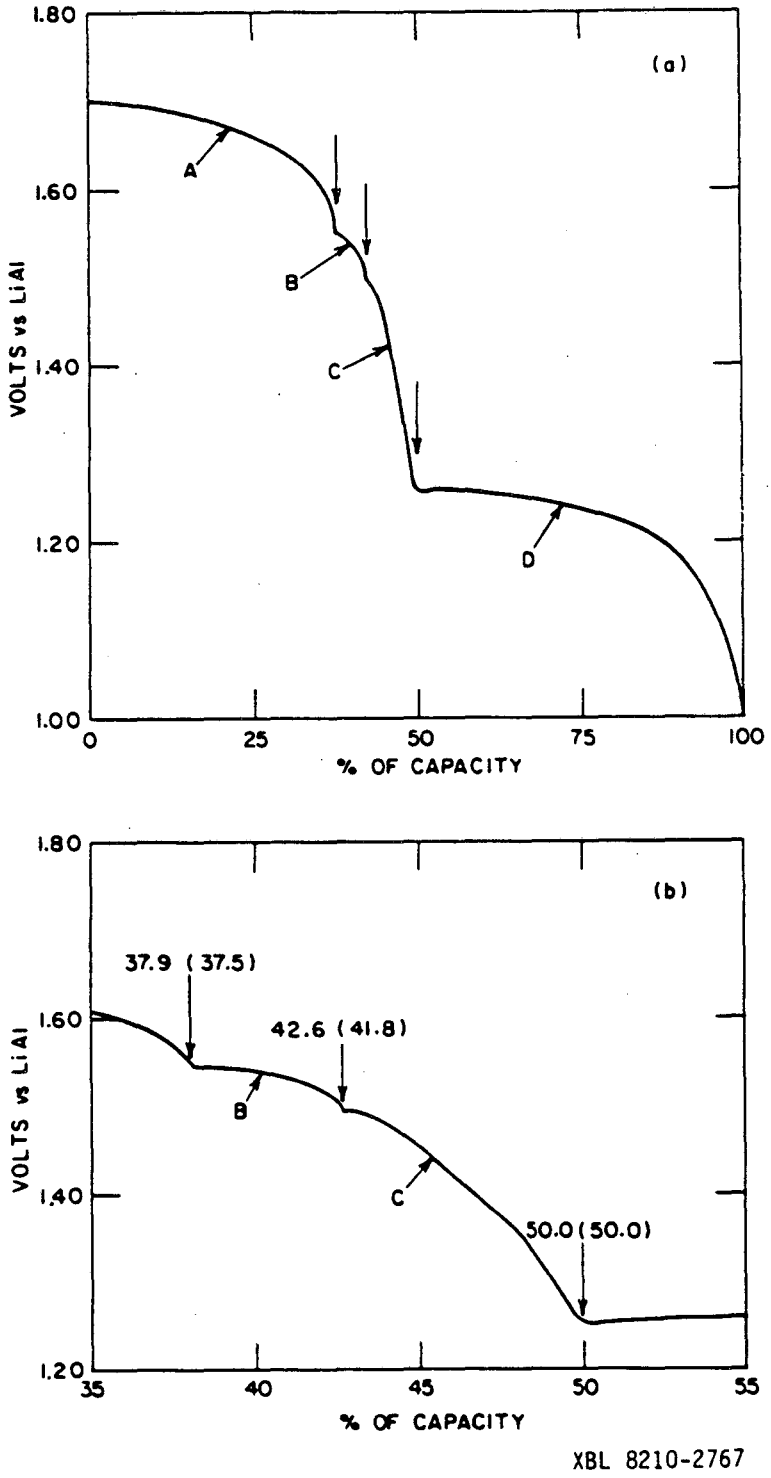

Figure 13. Discharge curve for an FeS_2 electrode, measured against a LiAl reference electrode, with LiCl-KCl eutectic electrolyte at 417°C and 12 mA/cm^2. The A, B, C, and D designations refer to the four observed electrochemical reactions. The arrows indicate the shift from one reaction to another. The percentages given above the arrows are the experimental values; those in parentheses are predicted from the Li-Fe-S phase diagram of Figure 4.

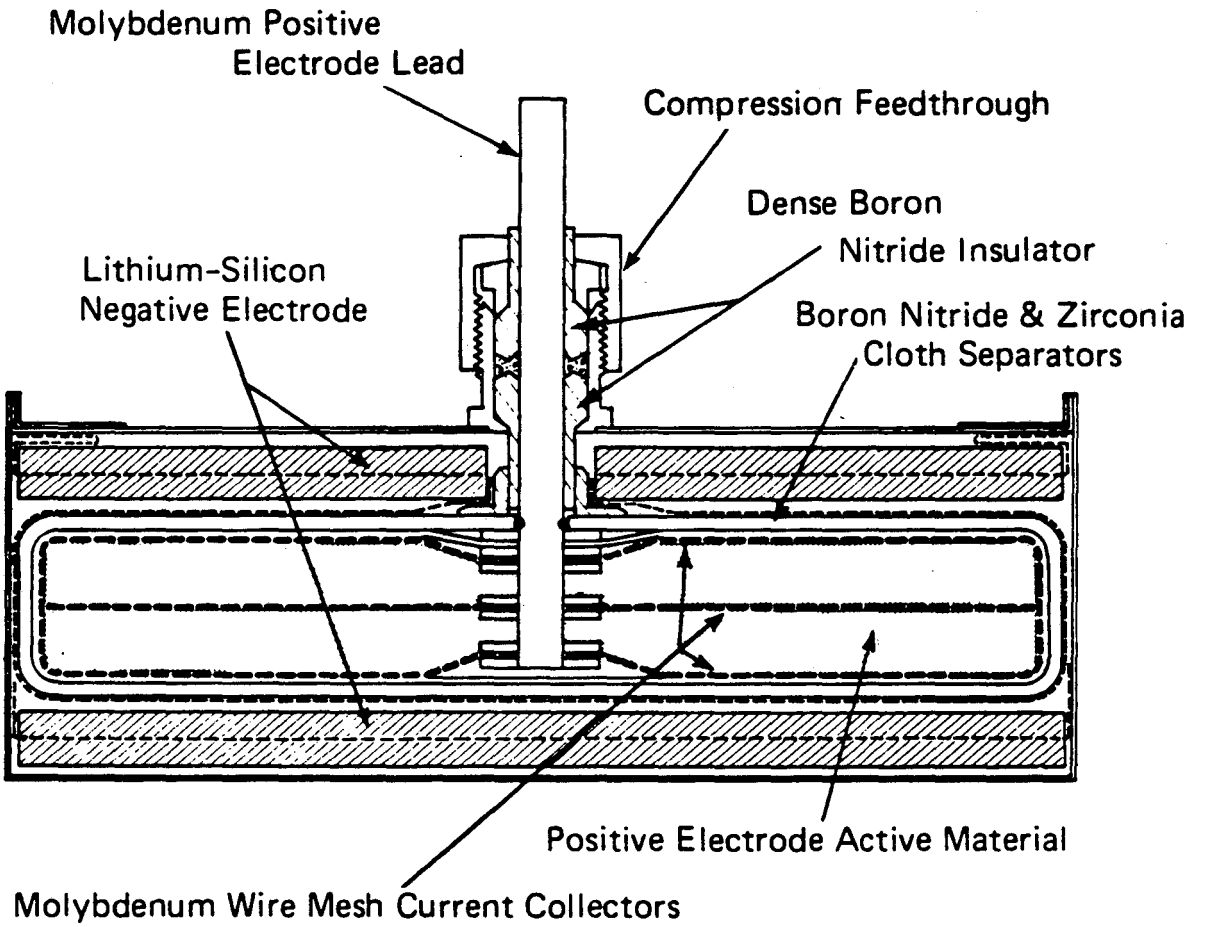

XBL 802-8075

Figure 14. Cross section of a disk-shaped Li_4Si/FeS_2 cell, having about 70-Ah capacity

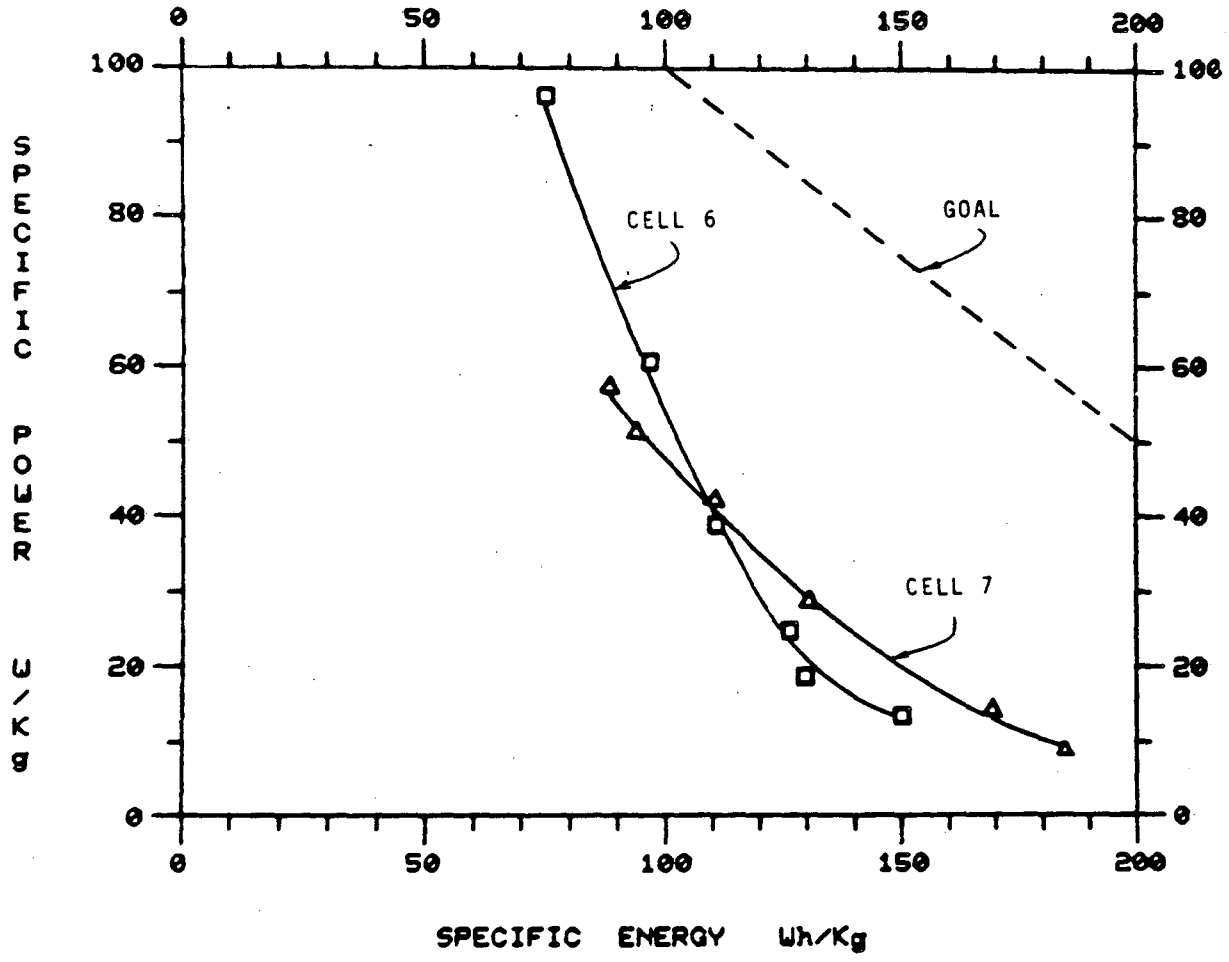

XBL 802-8065

Figure 15. Specific power vs. specific energy curves for Li_4Si-FeS_2 cells.

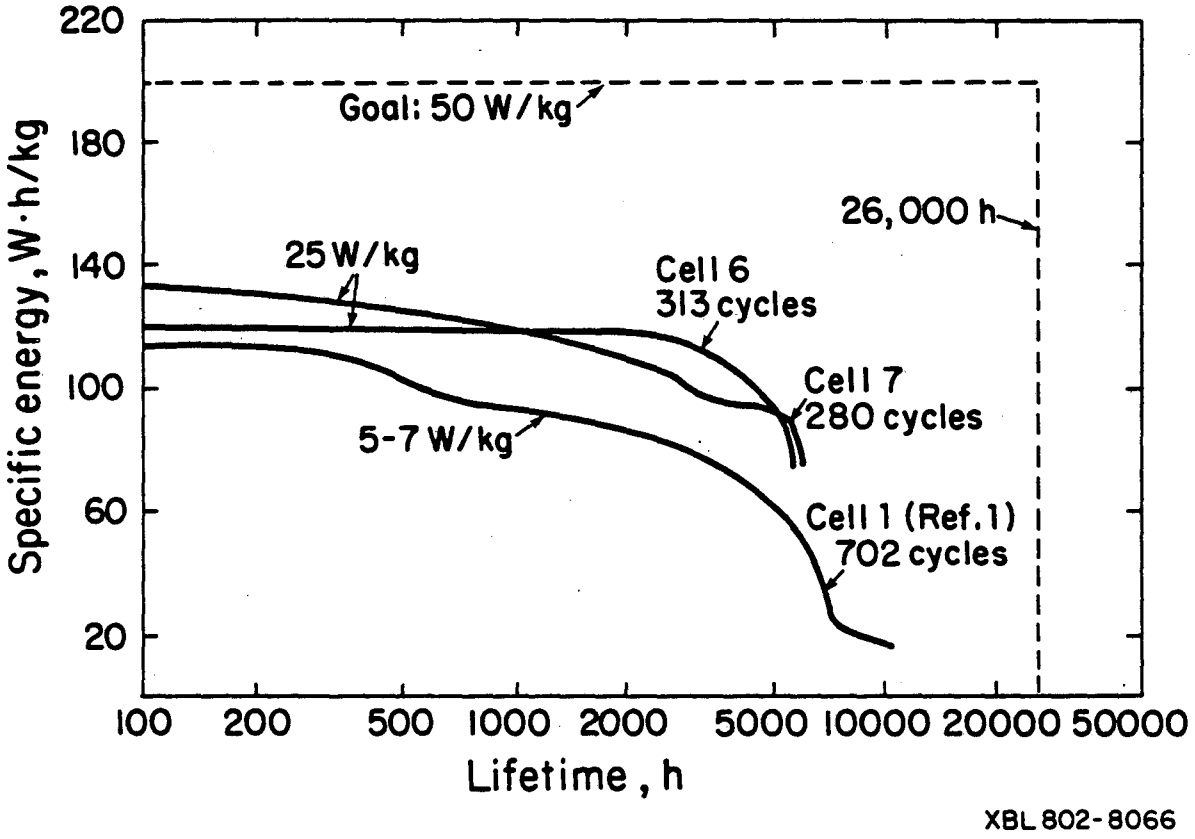

Figure 16. Specific energy vs. operating time curves for $LiAl/FeS_2$ and Li_4Si/FeS_2 cells.

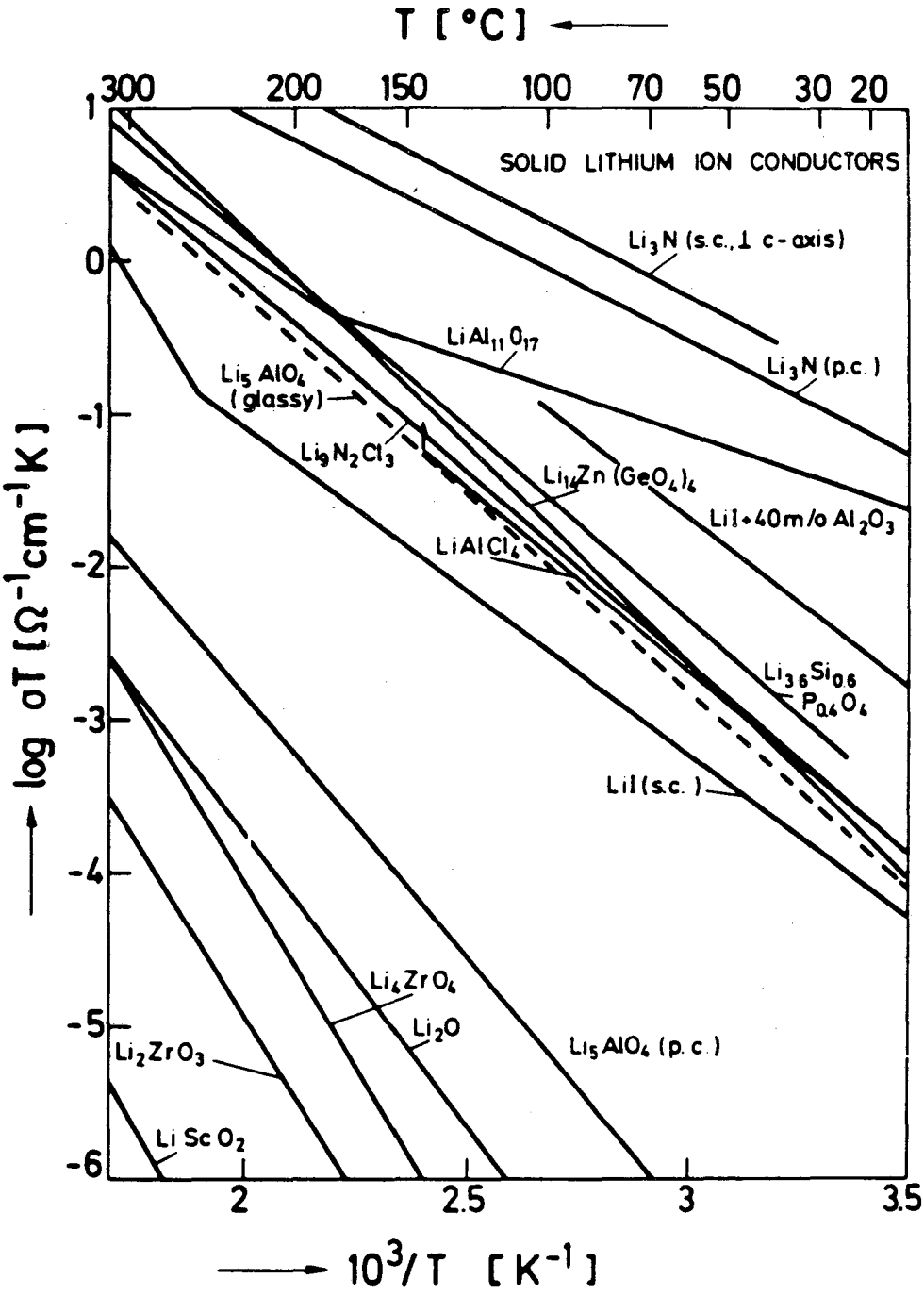

XBL 8210-2981

Figure 17. Conductivity of solid lithium ion conductors. The product of the conductivity σ and the absolute temperature T is plotted vs. the inverse absolute temperature.

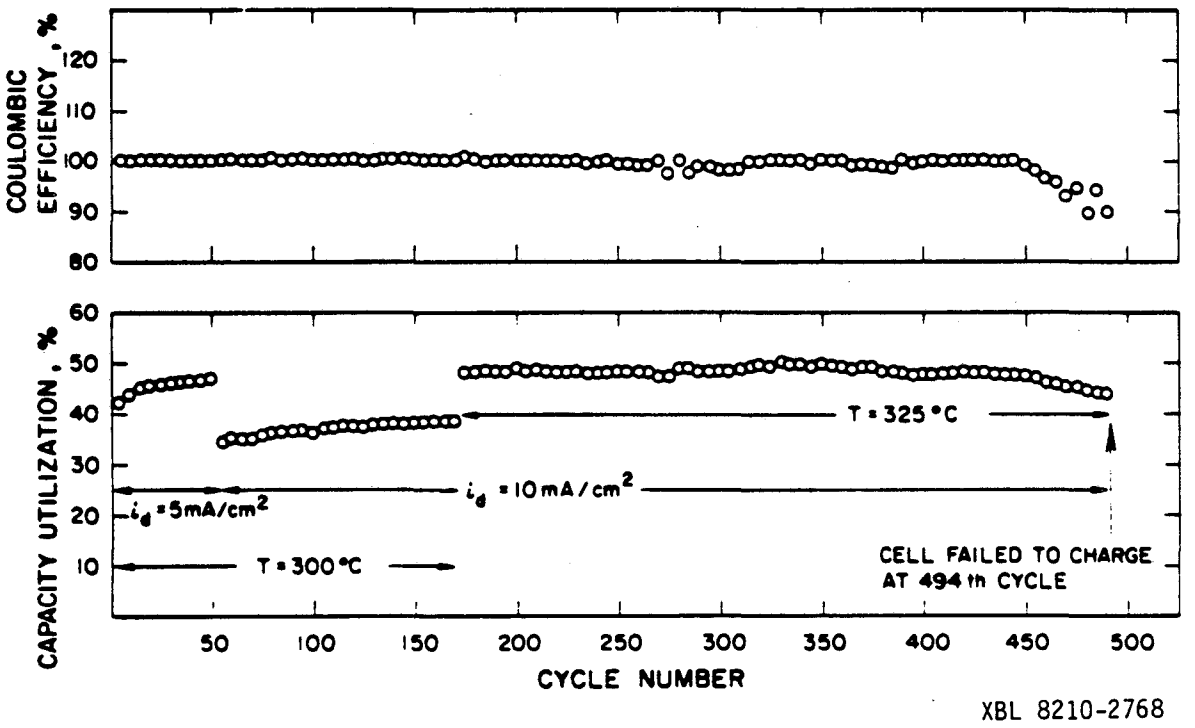

Figure 18. Performance of $Li_{3.74}Si/LiI\text{-}Al_2O_3/TiS_2$ cell. Charging rate = 5 mA/cm^2, i_d = discharge rate. Upper cutoff voltage = 2.3 V.

TECHNICAL INFORMATION DEPARTMENT
LAWRENCE BERKELEY LABORATORY
UNIVERSITY OF CALIFORNIA
BERKELEY, CALIFORNIA 94720